Available online at www.sciencedirect.com
ScienceDirect
Journal of Computational Physics 225 (2007) 753–770
JOURNAL OF COMPUTATIONAL PHYSICS
www.elsevier.com/locate/jcp

A hybrid-Vlasov model based on the current advance method for the simulation of collisionless magnetized plasma

F. Valentini [a,*], P. Trávníček [b], F. Califano [c], P. Hellinger [b], A. Mangeney [d]

[a] *Dipartimento di Fisica and CNISM, Universitá degli Studi della Calabria, Ponte P. Bucci, Cubo 31C, 87036 Arcavacata di Rende (CS), Italy*
[b] *Institute of Atmospheric Physics, AS CR, Prague, Czech Republic*
[c] *Dipartimento di Fisica and CNISM, Universitá di Pisa, Pisa, Italy*
[d] *LESIA – Observatoire de Paris, Section de Meudon 5, place Jules Janssen, 92195 Meudon Cedex, France*

Received 25 September 2006; received in revised form 28 December 2006; accepted 2 January 2007
Available online 10 January 2007

Abstract

We present a numerical scheme for the integration of the Vlasov–Maxwell system of equations for a non-relativistic plasma, in the hybrid approximation, where the Vlasov equation is solved for the ion distribution function and the electrons are treated as a fluid. In the Ohm equation for the electric field, effects of electron inertia have been retained, in order to include the small scale dynamics up to characteristic lengths of the order of the electron skin depth. The low frequency approximation is used by neglecting the time derivative of the electric field, i.e. the displacement current in the Ampere equation.

The numerical algorithm consists in coupling the splitting method proposed by Cheng and Knorr in 1976 [C.Z. Cheng, G. Knorr, J. Comput. Phys. 22 (1976) 330–351.] and the current advance method (CAM) introduced by Matthews in 1994 [A.P. Matthews, J. Comput. Phys. 112 (1994) 102–116.] In its present version, the code solves the Vlasov–Maxwell equations in a five-dimensional phase space (2-D in the physical space and 3-D in the velocity space) and it is implemented in a parallel version to exploit the computational power of the modern massively parallel supercomputers. The structure of the algorithm and the coupling between the splitting method and the CAM method (extended to the hybrid case) is discussed in detail. Furthermore, in order to test the hybrid-Vlasov code, the numerical results on propagation and damping of linear ion-acoustic modes and time evolution of linear elliptically polarized Alfvén waves (including the so-called whistler regime) are compared to the analytical solutions. Finally, the numerical results of the hybrid-Vlasov code on the parametric instability of Alfvén waves are compared with those obtained using a two-fluid approach.

PACS: 52.65.–y; 52.65.Ww; 52.25.Dg; 52.35.Fp; 52.35.Bj

Keywords: Vlasov; Hybrid; Splitting; CAM; EMHD; Alfvén waves; Parametric instability

* Corresponding author. Tel.: +39 0984 496129; fax: +39 0984 494401.
E-mail address: valentin@fis.unical.it (F. Valentini).

0021-9991/$ - see front matter
doi:10.1016/j.jcp.2007.01.001

1. Introduction

The understanding of the complex phenomena observed in natural and laboratory plasmas requires the use of numerical simulations. In many cases the collisional mean free path of particles is much longer than the typical scale lengths involved in these phenomena. Therefore, the plasma can be considered as collisionless and the Vlasov equation is used to investigate the behavior of the system. The most widely used method to describe numerically the kinetic dynamics of a plasma system is the particle in cell (PIC) method, essentially a Monte-Carlo method [3]. Nevertheless, Eulerian Vlasov codes, based on the direct numerical integration of the particle distribution function, have nowadays become largely adopted.

PIC codes represent historically the most adopted approach to numerical simulations of plasmas in the framework of the kinetic theory. PIC simulations follow the particle dynamics through a Lagrangian approach, i.e. integrating numerically the equation of motion for a large number of macro-particles, under the effect of the external electromagnetic fields and/or the self-consistent fields, i.e. the ones created by the particle dynamics itself. The distribution of particles is described in a statistical way where "real particles" are represented by so called super-particles. Each super-particle represents a given percentage of density and carries given amount of momentum. The density and momentum are distributed among macro-particles in such a way that their weighted summation at a given point of the spatial domain provides a mean value of the given moment of the particle distribution function with certain accuracy determined by the statistical properties of the set of macro-particles.

On the other hand, the Vlasov approach [4] is an Eulerian approach, where Vlasov equation is numerically solved by calculating the value of the particle distribution function at each time step on an uniform fixed grid used to sample the phase space. Moments needed for the time integration of the Maxwell equations are evaluated by straight numerical integration of the distribution function. Such Eulerian approach avoids the statistical noise caused by the fact that macro-particles in PIC codes represent values of the distribution function at randomly selected points of the phase space. It is necessary, however, to point out that the Eulerian Vlasov algorithm presents some limitations due to the large amount of computing resources and execution time needed to advance the distribution function.

To reduce these computational limitations, one can adopt several approximations to simplify the physical scenario, as the high frequency approximation that neglects the ion dynamics, or the hybrid approximation [2] where, for relatively large spatial scales and low frequencies, the detailed behavior of the electrons is irrelevant and the ions dominate the dynamics of the system. In the hybrid approximation, the ions are treated as kinetic particles whereas the electrons are represented as massless fluid. The hybrid scheme [2] was introduced to simplify the description of the electron dynamics, in order to eliminate their fast and small scale dynamics. As a consequence, larger time steps can be used, like fractions of the local inverse of the ion gyrofrequency Ω_{ci}^{-1} (typical for ion dynamics). However, in several problems (see, for example, study of reformation of one-dimensional perpendicular shocks [5]) the standard hybrid approximation is too restrictive and may lead to unphysical conclusions, since hybrid codes use a MHD framework where electrons are reduced to a massless, isothermal, isotropic fluid.

On the other hand, the electron inertial scales, not included by these numerical models, can be of crucial importance in many processes in different physical environments. For example, it is shown in [5] that the maximum gradient $\mathrm{d}B_y/\mathrm{d}x/B_0$ in the shock front simulated by the hybrid code without the capability of resolving the electron inertial scales strongly grows with decreasing spatial resolution $\mathrm{d}x$, while it is expected such growth to stop at the electron inertial scales. It is also known that the typical scale of the shock thickness and the typical scale of the upstream dispersive whistler wave trains is the electron inertial length c/ω_{pe} (where c is speed of light and ω_{pe} is electron plasma frequency). The electron inertial scales can be naturally introduced in a hybrid code by considering the Ohm's law in a more general form by keeping the electron mass as finite. For an introduction to the topic of a hybrid model, see [6,7] and for a more detailed description of the hybrid models with different approximation of the electron fluid, see [8].

In this paper we present a numerical code which combines a kinetic Vlasov description of ions with a fluid description for electrons, going from the MHD to the EMHD time and length scales. In particular, we use the current advance method with cyclic leapfrog (CAM-CL) for the calculation of electromagnetic fields intro-

duced by Matthews [2] and we investigate the ion Vlasov equation using Knorr's splitting scheme [1] extended to the electromagnetic case in [4].

In many situations, the understanding of the complex plasma dynamics requires to set up a model where the degree of realism can be even rather poor (for example simplified and or reduced geometry, etc.), but it allows one to isolate and study the physical processes underlying the system evolution. This is the typical case where the very low noise Eulerian Vlasov algorithms should be used instead of Lagrangian PIC codes. Indeed, a large class of physical problems can be successfully modelled in a phase space of lower dimensionality where Vlasov algorithms are extremely accurate in the analysis of kinetic effects (for example wave-particle interaction) or in the description of the tails of the particle distribution. Furthermore, the Vlasov approach allows for a clean description of the evolution of a single-mode perturbation, at variance with PIC codes where each possible mode in the simulation domain has got however a "small" amount of energy deriving from the statistical noise. Finally, a low noise algorithm is very useful also in the case of low amplitude initial perturbations problems, such as for instance the linear stage of instabilities, where the amplitude of each mode in the spectrum could be of the same order of the noise introduced by PIC codes. In this sense, Vlasov codes must be considered as complementary and not as an alternative to the PIC approach which is certainly the leading approach for the study of "realistic" problems.

The paper is organized as follows. Section 2 is devoted to a detailed overview of the Ohm's law, in the ideal magnetohydrodynamic (MHD) limit, in the Hall MHD limit (HMHD), and finally in the electron MHD limit (EMHD). In Section 3, the hybrid-Vlasov code is presented, and the numerical algorithm is described in detail. In Section 4, we summarize the structure of the algorithm and describe the discretization of the numerical domain. In Section 5, we discuss the propagation of linear ion-acoustic modes and the evolution of linear Alfvén waves, comparing the numerical results to the theoretical prediction, as a test for the numerical accuracy of the hybrid-Vlasov code. In Section 6, the parametric instability of Alfvén waves is reproduced numerically using the hybrid-Vlasov code and the numerical results are compared to those obtained with a two-fluid model. A short summary is presented in Section 7.

2. Ohm's law in MHD, HMHD and EMHD limits

In this section, we discuss the *Ohm's law*, which relates the electric field $\mathbf{E}(\mathbf{x},t)$ to the magnetic field $\mathbf{B}(\mathbf{x},t)$, the electric current $\mathbf{j}(\mathbf{x},t)$, the number density $n(\mathbf{x},t)$ of the plasma, the electron pressure $P_e(\mathbf{x},t)$ and the ion pressure $\Pi_{ij}(\mathbf{x},t)$. For small wavelengths and high frequencies, the one fluid ideal magnetohydrodynamics (MHD) description is no longer sufficient and it may be necessary to include the Hall effect (HMHD) and eventually electron inertia (EMHD). Then a two fluid theory (electron and ions) must be used where the more subtle electron effects have to be taken into account.

A general Ohm's law can be obtained for phenomena with typical frequencies ω and spatial scales l such that:

- Quasi-neutrality is satisfied: $l \gg \lambda_{\mathrm{D}_e}$, $\omega \ll \omega_{\mathrm{p}e}$.
- Displacement current is negligible.
- The plasma is weakly magnetized: $\Omega_{\mathrm{c}e} \ll \omega_{\mathrm{p}e}$.

Here, λ_{D_e} is the electron Debye length, $\omega_{\mathrm{p}e} = (4\pi ne^2/m_e)^{1/2}$ the electron plasma frequency, $\Omega_{\mathrm{c}e} = eB/m_e c$ the electron cyclotron frequency, e and m_e the electron electric charge (absolute value) and mass and c the speed of light.

We neglect the displacement current in the Ampere equation and assume quasi-neutrality:

$$ne(\mathbf{u}_i - \mathbf{u}_e) = \mathbf{j} = \frac{c}{4\pi}\nabla \times \mathbf{B}, \quad n_e \simeq n_i \equiv n \tag{1}$$

We also use the Faraday equation:

$$\frac{\partial \mathbf{B}}{\partial t} = -c\nabla \times \mathbf{E} \tag{2}$$

Electron and ion momentum equations read:

$$\frac{\partial(n\mathbf{u}_e)}{\partial t}+\nabla\cdot(n\mathbf{u}_e\mathbf{u}_e)=-\frac{1}{m_e}\nabla P_e-\frac{ne}{m_e}\left(\mathbf{E}+\frac{\mathbf{u}_e\times\mathbf{B}}{c}\right) \tag{3}$$

$$\frac{\partial(n\mathbf{u}_i)}{\partial t}+\nabla\cdot(n\mathbf{u}_i\mathbf{u}_i)=-\frac{1}{m_i}\nabla\cdot\boldsymbol{\Pi}+\frac{ne}{m_i}\left(\mathbf{E}+\frac{\mathbf{u}_i\times\mathbf{B}}{c}\right) \tag{4}$$

The left side of Eq. (3), using Eqs. (1) and (2) gives:

$$\frac{\partial(n\mathbf{u}_e)}{\partial t}=\frac{\partial(n\mathbf{u}_i)}{\partial t}-\frac{\partial}{\partial t}\left(\frac{\mathbf{j}}{e}\right)=\frac{\partial(n\mathbf{u}_i)}{\partial t}+\frac{c^2}{4\pi e}\nabla\times(\nabla\times\mathbf{E})$$

$$\nabla\cdot(n\mathbf{u}_e\mathbf{u}_e)=\nabla\cdot\left[n\left(\mathbf{u}_i-\frac{\mathbf{j}}{ne}\right)\left(\mathbf{u}_i-\frac{\mathbf{j}}{ne}\right)\right]=\nabla\cdot(n\mathbf{u}_i\mathbf{u}_i)-\frac{1}{e}\nabla\cdot(\mathbf{u}_i\mathbf{j})-\frac{1}{e}\nabla\cdot(\mathbf{j}\mathbf{u}_i)+\nabla\cdot\left(\frac{\mathbf{j}\mathbf{j}}{ne^2}\right)$$

By subtracting Eq. (3) from Eq. (4) and defining $\mu=1/m_e+1/m_i$ we get

$$\mu ne\mathbf{E}+\frac{c^2}{4\pi e}\nabla\times(\nabla\times\mathbf{E})=\frac{1}{m_i}\nabla\cdot\boldsymbol{\Pi}-\frac{1}{m_e}\nabla P_e+\frac{1}{m_e c}(\mathbf{j}\times\mathbf{B})-\frac{\mu ne}{c}(\mathbf{u}_i\times\mathbf{B})+\frac{1}{e}\nabla\cdot(\mathbf{u}_i\mathbf{j})+\frac{1}{e}\nabla\cdot(\mathbf{j}\mathbf{u}_i)-\nabla\cdot\left(\frac{\mathbf{j}\mathbf{j}}{ne^2}\right)$$

This equation does not have time derivatives, as a consequence of the quasi-neutrality assumption. From now the ion velocity will be indicated without the index i, i.e. $\mathbf{u}_i\to\mathbf{u}$. Assuming $\mu\simeq 1/m_e$, the above equation becomes:

$$\mathbf{E}+\frac{m_e c^2}{4\pi ne^2}\nabla\times(\nabla\times\mathbf{E})=-\frac{1}{c}(\mathbf{u}\times\mathbf{B})+\frac{1}{nec}(\mathbf{j}\times\mathbf{B})+\frac{m_e}{nem_i}\nabla\cdot\boldsymbol{\Pi}-\frac{1}{ne}\nabla P_e+\frac{m_e}{ne^2}\nabla\cdot[\mathbf{u}\mathbf{j}+\mathbf{j}\mathbf{u}]-\frac{m_e}{ne^3}\nabla\cdot\left(\frac{\mathbf{j}\mathbf{j}}{n}\right) \tag{5}$$

where

$$\nabla\cdot[\mathbf{u}\mathbf{j}+\mathbf{j}\mathbf{u}]=\frac{\partial}{\partial x_j}[u_i j_j+j_i u_j];\quad \nabla\cdot\left(\frac{\mathbf{j}\mathbf{j}}{n}\right)=\frac{\partial}{\partial x_j}\left(\frac{j_i j_j}{n}\right)$$

We use the following characteristic quantities:

$$\bar{u}=u_{\mathrm{A}};\quad \bar{\omega}=\Omega_{\mathrm{ci}};\quad \bar{l}=u_{\mathrm{A}}/\Omega_{\mathrm{ci}}=c/\omega_{\mathrm{pi}}=d_i;\quad \bar{n};\quad \omega_{\mathrm{pi}}=4\pi\bar{n}e^2/m_i;\quad \omega_{\mathrm{pe}}=4\pi\bar{n}e^2/m_e;$$
$$\overline{P}_{p/e}=\bar{n}m_i u_{\mathrm{A}}^2;\quad \overline{E}=m_i u_{\mathrm{A}}\Omega_{\mathrm{ci}}/e;\quad \overline{B}=m_i c\Omega_{\mathrm{ci}}/e \tag{6}$$

Here, u_{A} is the Alfvén velocity, Ω_{ci} and $\omega_{\mathrm{p}i}$ the ion cyclotron and the ion plasma frequencies, respectively and d_i the ion skin depth. The electron skin depth, in units of d_i (i.e. in dimensionless units) is given by the square root of the mass ratio, $d_e=\sqrt{(m_e/m_i)}$. Taking into account quasi-neutrality condition ($\nabla\cdot\mathbf{E}=0$), we obtain $\nabla\times(\nabla\times\mathbf{E})=-\Delta\mathbf{E}$. Then, Ohm's law reads:

$$\mathbf{E}-\frac{d_e^2}{n}\Delta\mathbf{E}=-(\mathbf{u}\times\mathbf{B})+\frac{1}{n}(\mathbf{j}\times\mathbf{B})+\frac{1}{n}d_e^2\nabla\cdot\boldsymbol{\Pi}-\frac{1}{n}\nabla P_e+\frac{d_e^2}{n}\nabla\cdot[\mathbf{u}\mathbf{j}+\mathbf{j}\mathbf{u}]-\frac{1}{n}d_e^2\nabla\cdot\left(\frac{\mathbf{j}\mathbf{j}}{n}\right) \tag{7}$$

where now all the quantities are dimensionless.

In the limit of long wavelength $\bar{l}\gg c/\omega_{\mathrm{p}i}$, low frequency $\bar{\omega}\ll\Omega_{ci}$, the plasma dynamics can be described by "Ideal" MHD, where electrons contribute only to the total pressure and maintain charge neutrality; in these conditions, the Ohm's law can be written as follows:

$$\mathbf{E}+\mathbf{u}\times\mathbf{B}=0 \tag{8}$$

When the typical wavelength becomes comparable to the ion inertia scale, it is necessary to retain the Hall term, which generates an electric field from the component of the electric current perpendicular to the magnetic field; the Ohm equation, in the HMHD limit, reads:

$$\left(\mathbf{E}+\mathbf{u}\times\mathbf{B}-\frac{\mathbf{j}\times\mathbf{B}}{n}\right)+\frac{1}{n}\nabla P_e=0 \tag{9}$$

When the electron effects begin to play a non-negligible role, i.e. the electron dynamics starts to decouple from the ion dynamics, the full equation (7) has to be used. The electric field is no longer given by an algebraic

expression but by a partial differential equation. As usual, we neglect density fluctuations in the inertial LHS correction term in Eq. (7), $1/nd_e^2\Delta\mathbf{E} \sim d_e^2\Delta\mathbf{E}$ (where $\langle n\rangle = 1$ in dimensionless units), which is formally correct only in the strong guide field limit. Therefore, in a more compact form, Eq. (7) can be written as an Helmoltz equation, by a simple manipulation:

$$(1 - d_e^2\Delta)\mathbf{E} = \mathbf{S} \tag{10}$$

where

$$\mathbf{S} = -\mathbf{u}\times\mathbf{B} + \frac{\mathbf{j}\times\mathbf{B}}{n} + \frac{1}{n}\nabla\cdot\boldsymbol{\Pi}^{\mathrm{T}} + \frac{\boldsymbol{\Sigma}}{n}, \tag{11}$$

$$\Pi_{ij}^{\mathrm{T}} = d_e^2\Pi_{ij} - P_e\delta_{ij} - \frac{d_e^2}{n}(\nabla\times\mathbf{B})_i(\nabla\times\mathbf{B})_j \tag{12}$$

The additional term contains corrections of order $d_e^2/\bar{l}^2$:

$$\Sigma_i = d_e^2\frac{\partial}{\partial x_j}\left[u_i(\nabla\times\mathbf{B})_j + u_j(\nabla\times\mathbf{B})_i\right] \tag{13}$$

This general Ohm's law contains the *electron magnetohydrodynamics* limit [9] which has been developed to describe phenomena at frequencies ω large compared to the ion gyro and plasma frequencies, but below the electron gyro and plasma frequencies and scales smaller but of the order of the electron skin depth $l \ll c/\omega_{\mathrm{pe}}$ and larger than the Debye length λ_{D_e}. With this ordering, ion motions are negligible and the dynamics is governed by the electrons. In particular, the current is carried by the electrons only, $\mathbf{j} = -en_e\mathbf{v}_e$. Usually EMHD is considered to imply incompressible motions, which is valid only under the conditions: (i) $\omega \ll \omega_{\mathrm{pe}}$, (ii) $l \gg \lambda_{D_e}$ and finally, (iii) $(d_e^2/l^2)(\Omega_{\mathrm{ce}}^2/\omega_{\mathrm{pe}}^2) \ll 1$, i.e. either a weakly magnetized plasma or very small scale lengths.

3. Hybrid-Vlasov code

The normalized equations used in our model (see Eq. (6) for characteristic quantities) are the following:

(1) The *Vlasov equation* for the ion distribution function $f(\mathbf{x},\mathbf{v},t)$

$$\frac{\partial f}{\partial t} + \mathbf{v}\cdot\nabla f + (\mathbf{E} + \mathbf{v}\times\mathbf{B})\cdot\frac{\partial f}{\partial \mathbf{v}} = 0 \tag{14}$$

(2) The *Ohm's law* for the electric field

$$\mathbf{E} - d_e^2\Delta\mathbf{E} = -(\mathbf{u}\times\mathbf{B}) + \frac{1}{n}(\mathbf{j}\times\mathbf{B}) + \frac{1}{n}d_e^2\nabla\cdot\boldsymbol{\Pi} - \frac{1}{n}\nabla P_e + \frac{d_e^2}{n}\nabla\cdot[\mathbf{uj} + \mathbf{ju}] - \frac{1}{n}d_e^2\nabla\cdot\left(\frac{\mathbf{jj}}{n}\right) \tag{15}$$

Here, the ion density n, the ion bulk velocity $\mathbf{u}$ and the ion pressure tensor $\boldsymbol{\Pi}$ are obtained as the moments of the ion distribution function f:

$$n(\mathbf{x},t) = \int f(\mathbf{x},\mathbf{v},t)\,\mathrm{d}\mathbf{v}, \tag{16}$$

$$n\mathbf{u}(\mathbf{x},t) = \int \mathbf{v}f(\mathbf{x},\mathbf{v},t)\,\mathrm{d}\mathbf{v}, \tag{17}$$

$$\boldsymbol{\Pi}(\mathbf{x},t) = \int (\mathbf{v}-\mathbf{u})(\mathbf{v}-\mathbf{u})f(\mathbf{x},\mathbf{v},t)\,\mathrm{d}\mathbf{v} \tag{18}$$

The electron pressure P_{e} is considered a function of the density $n = n_e = n_i$, as, for example, in the isothermal approximation $P_e = nk_{\mathrm{B}}T_e$, where T_e is the electron temperature. The choice of the appropriate Ohm's law depends on the problem we intend to solve (cf. previous section); however in all cases the electric field is evaluated via the Ohm's law at a given point of the simulation loop.

(3) Maxwell equations, for the magnetic field $\mathbf{B}$

$$\frac{\partial\mathbf{B}}{\partial t} = -\nabla\times\mathbf{E}, \quad \nabla\times\mathbf{B} = \mathbf{j} \tag{19}$$

Since we are using the low frequency approximation, corresponding to neglect the time derivative of the electric field in the Ampere equation, the electric current $\mathbf{j} = e(\mathbf{j}_i - \mathbf{j}_e)$ is determined by the magnetic field gradients.

As discussed in Section 1, to solve our hybrid-Vlasov system numerically we shall use the current advance method (CAM) coupled to the splitting method. The CAM method provides the second order numerical solution for the advancement of electric and magnetic fields, while the splitting method is a second order scheme in time for the advance of the particle distribution function in phase space. The accuracy in Δx and Δv (the mesh size of the spatial grid and the velocity grid, respectively) depends on the interpolation algorithm used to evaluate the distribution function on the grid points at each time step.

3.1. The splitting method

The splitting algorithm in our case applies as follows. Let us denote by $\Lambda_x(t)F(\mathbf{x},\mathbf{v})$ and $\Lambda_v(t)F(\mathbf{x},\mathbf{v})$ the solutions at time t of the two equations:

$$\frac{\partial f}{\partial t} + \mathbf{v}\cdot\nabla f = 0 \tag{20}$$

$$\frac{\partial f}{\partial t} + (\mathbf{E} + \mathbf{v}\times\mathbf{B})\cdot\frac{\partial f}{\partial \mathbf{v}} = 0 \tag{21}$$

with the initial condition $f(\mathbf{x},\mathbf{v},t=0) = F(\mathbf{x},\mathbf{v})$. In the first equation, the velocity $\mathbf{v}$ is considered as a parameter, while in the second it is the space variable $\mathbf{x}$ and the electric and magnetic fields $\mathbf{E}$ and $\mathbf{B}$ which are treated as parameters.

The splitting scheme provides a second order accurate in time solution at $t_N = N\Delta t$ to Eq. (14) in the form

$$f(\mathbf{x},\mathbf{v},t_N) = \left[\Lambda_x\left(\frac{\Delta t}{2}\right)\Lambda_v(\Delta t)\Lambda_x\left(\frac{\Delta t}{2}\right)\right]^N f(\mathbf{x},\mathbf{v},0) \tag{22}$$

The explicit expressions for the operators Λ_x and Λ_v, in the electromagnetic case, have been obtained by Mangeney et al. in 2002 [4], in the case of cartesian numerical grids in phase space (see also [10–20] for detailed discussions on the numerical integration of hyperbolic equations). As we shall see later, the numerical integration of the magnetic field equation (19) by the CAM method requires the evaluation of the distribution function at half time steps $t_N + \Delta t/2$. In the following, we will use the notation f^* for the space advanced distribution function (by the operator Λ_x) and $\tilde{f}$ for the velocity advanced distribution function (by the operator Λ_v).

First of all, we discuss the initial setup of the numerical integration by starting from the initial condition at $t = 0$, where all the fields and the distribution function are given. Starting from the initial condition, we advect the distribution function by a half time step in the physical space:

$$f^*(\mathbf{x},\mathbf{v},\Delta t/2) = \Lambda_x(\Delta t/2)f(\mathbf{x},\mathbf{v},0) \tag{23}$$

The value of the electric and magnetic fields at $t = \Delta t/2$, $\mathbf{E}(\mathbf{x},\Delta t/2)$ and $\mathbf{B}(\mathbf{x},\Delta t/2)$, can be calculated by using any explicit scheme in time starting from the initial condition $\mathbf{E}(\mathbf{x},0)$ and $\mathbf{B}(\mathbf{x},0)$. Then, using $\mathbf{E}(\mathbf{x},\Delta t/2)$ and $\mathbf{B}(\mathbf{x},\Delta t/2)$, we can advance the distribution function in the velocity space by a integer time step:

$$\tilde{f}(\mathbf{x},\mathbf{v},\Delta t) = \Lambda_v(\Delta t)f^*(\mathbf{x},\mathbf{v},\Delta t/2) \tag{24}$$

Once we initialized the numerical integration as described above, a generic time step from t to $t + \Delta t$ can be summarized as follows. Suppose the quantities $f^*(\mathbf{x},\mathbf{v},t-\Delta t/2)$, $\mathbf{E}(\mathbf{x},t-\Delta t/2)$, $\mathbf{B}(\mathbf{x},t-\Delta t/2)$ and $\tilde{f}(\mathbf{x},\mathbf{v},t)$ are given; then we advance the distribution in the physical space by a integer time step:

$$f^*(\mathbf{x},\mathbf{v},t+\Delta t/2) = \Lambda_x(\Delta t)\tilde{f}(\mathbf{x},\mathbf{v},t) \tag{25}$$

Using the CAM method described in the next section, we can calculate the fields $\mathbf{E}(\mathbf{x},t+\Delta t/2)$, $\mathbf{B}(\mathbf{x},t+\Delta t/2)$ and finally advance the distribution in the velocity space by a integer time step:

$$\tilde{f}(\mathbf{x},\mathbf{v},t+\Delta t)=\Lambda_v(\Delta t)f^*(\mathbf{x},\mathbf{v},t+\Delta t/2) \tag{26}$$

3.2. Current advance method for fields

We now describe the way to extend the current advance method for the electromagnetic fields to the case of hybrid approximation (HCAM). The sources needed to obtain the fields **E** and **B** at $t+\Delta t/2$ are the ion density $n(\mathbf{x},t+\Delta t/2)$, the flux $\mathbf{j}(\mathbf{x},t+\Delta t/2)$ and the ion pressure tensor $\Pi_{ij}(\mathbf{x},t+\Delta t/2)$, starting from the known quantities

$$n^*(\mathbf{x},t+\Delta t/2)=\int f^*(\mathbf{x},\mathbf{v},t+\Delta t/2)\,\mathrm{d}\mathbf{v}, \tag{27}$$

$$\mathbf{j}^*(\mathbf{x},t+\Delta t/2)=\int \mathbf{v}f^*(\mathbf{x},\mathbf{v},t+\Delta t/2)\,\mathrm{d}\mathbf{v}, \tag{28}$$

$$\boldsymbol{\Pi}^*(\mathbf{x},t+\Delta t/2)=\int (\mathbf{v}-\mathbf{u})(\mathbf{v}-\mathbf{u})f^*(\mathbf{x},\mathbf{v},t+\Delta t/2)\,\mathrm{d}\mathbf{v} \tag{29}$$

and

$$\tilde{n}(\mathbf{x},t)=\int \tilde{f}(\mathbf{x},\mathbf{v},t)\,\mathrm{d}\mathbf{v}, \tag{30}$$

$$\tilde{\mathbf{j}}(\mathbf{x},t)=\int \mathbf{v}\tilde{f}(\mathbf{x},\mathbf{v},t)\,\mathrm{d}\mathbf{v}, \tag{31}$$

$$\tilde{\boldsymbol{\Pi}}(\mathbf{x},t)=\int (\mathbf{v}-\mathbf{u})(\mathbf{v}-\mathbf{u})\tilde{f}(\mathbf{x},\mathbf{v},t)\,\mathrm{d}\mathbf{v} \tag{32}$$

It is worth to underline that, starting from $f^*(\mathbf{x},\mathbf{v},t+\Delta t/2)$, the *real* distribution function at $t+\Delta t/2$ would be

$$f(\mathbf{x},\mathbf{v},t+\Delta t/2)=\Lambda_v(\Delta t/2)f^*(\mathbf{x},\mathbf{v},t+\Delta t/2) \tag{33}$$

Of course, this supplementary advance of the distribution needed to compute the moments $n(\mathbf{x},t+\Delta t/2)$, $\mathbf{j}(\mathbf{x},t+\Delta t/2)$ and $\Pi_{ij}(\mathbf{x},t+\Delta t/2)$ would be extremely time consuming as the numerical advancement of the distribution function through the operators Λ_x and Λ_v takes most of the computational time. However, this supplementary advancement is avoided by our coupling of the splitting and CAM methods.

To advance the magnetic field from $t-\Delta t/2$ to $t+\Delta t/2$ second order accurate in time

$$\mathbf{B}\left(\mathbf{x},t+\frac{\Delta t}{2}\right)=\mathbf{B}\left(\mathbf{x},t-\frac{\Delta t}{2}\right)-\Delta t[\nabla\times\mathbf{E}(\mathbf{x},t)] \tag{34}$$

we only need to evaluate the electric field $\mathbf{E}(\mathbf{x},t)$ at integer time steps first order accurate in time. This can be done by calculating the particle moments $n^{(1)},\boldsymbol{j}^{(1)}$ and $\boldsymbol{\Pi}^{(1)}$ at time t, also accurate to first order in time. This is done by noting that the first order accurate *real* distribution function at time t can be approximated by

$$f(\mathbf{x},\mathbf{v},t)=\Lambda_x\left(\frac{\Delta t}{2}\right)\tilde{f}(\mathbf{x},\mathbf{v},t)\sim\left\{1-\frac{\Delta t}{2}(\mathbf{v}\cdot\nabla)\right\}\tilde{f}(\mathbf{x},\mathbf{v},t) \tag{35}$$

In the same way, the space advanced distribution function f^* accurate to first order at time $t+\Delta t/2$ can be approximated as

$$f^*\left(\mathbf{x},\mathbf{v},t+\frac{\Delta t}{2}\right)=\Lambda_x(\Delta t)\tilde{f}(\mathbf{x},\mathbf{v},t)\sim\{1-\Delta t(\mathbf{v}\cdot\nabla)\}\tilde{f}(\mathbf{x},\mathbf{v},t) \tag{36}$$

Manipulating the two previous equations for $f(\mathbf{x},\mathbf{v},t)$ and $f^*(\mathbf{x},\mathbf{v},t+\Delta t/2)$ one realizes that $f(\mathbf{x},\mathbf{v},t)$ correct up to first order in Δt is given by the mean value between $\tilde{f}(\mathbf{x},\mathbf{v},t)$ and $f^*(\mathbf{x},\mathbf{v},t+\Delta t/2)$, i.e.

$$f(\mathbf{x},\mathbf{v},t)=\frac{1}{2}\left[\tilde{f}(\mathbf{x},\mathbf{v},t)+f^*\left(\mathbf{x},\mathbf{v},t+\frac{\Delta t}{2}\right)\right]$$

Therefore,

$$n^{(1)}(\mathbf{x},t)=\frac{1}{2}\left[n^*\left(\mathbf{x},t+\frac{\Delta t}{2}\right)+\tilde{n}(\mathbf{x},t)\right],$$
$$\mathbf{j}^{(1)}(\mathbf{x},t)=\frac{1}{2}\left[\mathbf{j}^*\left(\mathbf{x},t+\frac{\Delta t}{2}\right)+\tilde{\mathbf{j}}(\mathbf{x},t)\right],$$
$$\boldsymbol{\Pi}^{(1)}(\mathbf{x},t)=\frac{1}{2}\left[\boldsymbol{\Pi}^*\left(\mathbf{x},t+\frac{\Delta t}{2}\right)+\widetilde{\boldsymbol{\Pi}}(\mathbf{x},t)\right]$$

To complete the calculation of the electric field $\mathbf{E}(\mathbf{x},t)$, we have to evaluate the magnetic field $\mathbf{B}(\mathbf{x},t)$ needed in the Ohm's law. This can be done using the electric field at $t-\Delta t/2$.

$$\mathbf{B}(\mathbf{x},t)=\mathbf{B}(\mathbf{x},t-\Delta t)-\Delta t\left[\nabla\times\mathbf{E}\left(\mathbf{x},t-\frac{\Delta t}{2}\right)\right]$$

Once we have calculated $\mathbf{E}(\mathbf{x},t)$, we obtain $\mathbf{B}(\mathbf{x},t+\Delta t/2)$ using Eq. (34). In order to finally perform the velocity advance (26), we need the electric field $\mathbf{E}(\mathbf{x},t+\Delta t/2)$. It can be evaluated in the following way. To obtain the first order accurate *real* distribution function at $t+\Delta t/2$ starting from the known quantity $f^*(\mathbf{x},\mathbf{v},t+\Delta t/2)$, one has to solve the Eq. (21) over a halftime step $\Delta t/2$ using $f^*(\mathbf{x},\mathbf{v},t+\Delta t/2)$ as initial condition:

$$\frac{\partial f}{\partial t}+(\mathbf{E}^*+\mathbf{v}\times\mathbf{B}^*)\cdot\frac{\partial f}{\partial\mathbf{v}}=0 \tag{37}$$

where $\mathbf{B}^*=\mathbf{B}(\mathbf{x},t+\Delta t/2)$ and $\boldsymbol{E}^*$ is the electric field evaluated at $t+\Delta t/2$ from the Ohm's law using $n^*(\mathbf{x},t+\Delta t/2)$, $\mathbf{j}^*(\mathbf{x},t+\Delta t/2)$, $\boldsymbol{\Pi}^*(\mathbf{x},t+\Delta t/2)$ and $\boldsymbol{B}^*$.

Taking the zero and first order moments from Eq. (37), one obtains:

$$\frac{\partial n}{\partial t}=0\Rightarrow n(\mathbf{x},t+\Delta t/2)=n^*(\mathbf{x},t+\Delta t/2) \tag{38}$$

and

$$\frac{\partial j_i}{\partial t}=(n^*E_i^*+\epsilon_{ilm}j_l^*B_m^*) \tag{39}$$

where ϵ_{ilm} is the Levi–Civita permutation symbol. The previous equation can be solved to the first order to give:

$$j_i(\mathbf{x},t+\Delta t/2)=j_i^*(\mathbf{x},t+\Delta t/2)+\frac{\Delta t}{2}[n^*E_i^*+\epsilon_{ilm}j_l^*B_m^*]$$

We need more complicated manipulation of Eq. (37) for the ion pressure tensor Π_{ij}. Multiplying both sides of this equation by v_iv_j and integrating in the velocities, one obtains

$$\frac{\partial}{\partial t}\langle v_iv_j\rangle-(E_i^*j_j^*+E_j^*j_i^*)-\epsilon_{ilm}B_m^*\langle v_lv_m\rangle-\epsilon_{jlm}B_m^*\langle v_lv_m\rangle=0 \tag{40}$$

By defining $\mathbf{v}=\mathbf{w}+\mathbf{u}$, we get

$$\langle v_iv_j\rangle=\langle(w_i+u_i)(w_j+u_j)\rangle=\Pi_{ij}+\frac{j_ij_j}{n}$$

Using the previous expression and taking into account that we solve Eq. (21) over a halftime step $\Delta t/2$ with $f^*(\mathbf{x},\mathbf{v},t+\Delta t/2)$ as initial condition, Eq. (40), can be written as

$$\frac{\partial}{\partial t}\Pi_{ij}=\epsilon_{ilm}B_m^*\Pi_{lj}^*+\epsilon_{jlm}B_m^*\Pi_{li}^* \tag{41}$$

where Eq. (39) has been used. This differential equation for Π_{ij} is solved to first order by

$$\Pi_{ij}(\mathbf{x},t+\Delta t/2),=\Pi_{ij}^*(\mathbf{x},t+\Delta t/2)+\frac{\Delta t}{2}(\epsilon_{ilm}B_m^*\Pi_{lj}^*+\epsilon_{jlm}B_m^*\Pi_{li}^*)$$

At this point, we can evaluate the electric field $\mathbf{E}(\mathbf{x}, t + \Delta/2)$ through the Ohm's law using the quantities $n(\mathbf{x}, t + \Delta t/2)$, $\mathbf{j}(\mathbf{x}, t + \Delta t/2)$, $\boldsymbol{\Pi}(\mathbf{x}, t + \Delta t/2)$ and $\mathbf{B}(\mathbf{x}, t + \Delta t/2)$ calculated through the CAM method and finally advance the distribution function in the velocity space, according to Eq. (26).

To close this section, a few words about the numerical integration of the Ohm's law are in order. As it easy to see from Eq. (7), the inclusion of electron inertia causes an increasing of the computational effort, since, while Eqs. (8) and (9) are algebraic equations, Eq. (7) is a partial differential equation. This equation, for periodic boundary conditions in the physical space, can be solved using standard Fast Fourier Transform algorithms. On the other hand, when using open boundary conditions, we need to use (compact) finite difference schemes, which require the inversion of tridiagonal matrices. However, in both cases, the computational cost is negligible with respect to that needed to integrate the Vlasov equation. If also density fluctuations must be retained in the LHS correction term in Eq. (7), an iterative solver must be used which, however, should rapidly converge to the solution since it starts from a very good initial guess, i.e. from the solution at $t - \mathrm{d}t$.

4. Algorithm and code design

From the mathematical description presented in the previous section, we can easily summarize the structure of the algorithm of the hybrid-Vlasov code as follows:

(1) From $\tilde{f}$ calculate and memorize moments $\tilde{n}$, $\tilde{\mathbf{j}}$ and $\widetilde{\boldsymbol{\Pi}}$.
(2) Evaluate $f^* = \Lambda_x \tilde{f}$, then calculate the moments n^*, $\boldsymbol{j}^*$ and $\boldsymbol{\Pi}^*$.
(3) Evaluate the fields $\mathbf{E}$ and $\mathbf{B}$, using the CAM method (see Section 3.2).
(4) Advance the distribution function in the velocity domain $\tilde{f} = \Lambda_v f^*$.
(5) Use the previously described steps repeatedly to advance the calculation in time.

To complete the algorithm description, a few words are in order about the discretization of the numerical phase space domain. Here, we will limit our discussion to the Vlasov equation for the case of a five-dimensional phase space (x, y, v_x, v_y, v_z), where (x, y) are the spatial coordinates in a cartesian reference frame and (v_x, v_y, v_z) the velocity coordinates. Indeed, at the moment the full six-dimensional case, while being in principle a straightforward extension of the five-dimensional one, could be solved only with a numerical resolution too small to be of interest for plasma physics research. Periodic boundary conditions are used in the physical plane (x, y), while in the velocity space the distribution function is set to zero outside the numerical domain.

For the integration of the Vlasov equation, we use a uniform grid with $N_x \times N_y$ mesh points in physical space and $(2Nv_x + 1) \times (2Nv_y + 1) \times (2Nv_z + 1)$ points in velocity space covering the five-dimensional numerical domain $0 \leqslant x \leqslant L_x$, $0 \leqslant y \leqslant L_y$, $-v_x^{\max} \leqslant v_x \leqslant v_x^{\max}$, $-v_y^{\max} \leqslant v_y \leqslant v_y^{\max}$, $-v_z^{\max} \leqslant v_z \leqslant v_z^{\max}$. The corresponding distribution function $f(N_x, N_y, -Nv_x : Nv_x, -Nv_y : Nv_y, -Nv_z : Nv_z)$ is by far the largest data structure and its time advance uses repeatedly, both for the spatial and the velocity advance, the translation operators Λ_x and Λ_v (see Eqs. (20) and (21)), which corresponds in practice to an interpolation formula.

As discussed in Section 1, the computational effort required to solve the Vlasov–Maxwell system of equations is significant and today such simulations could only be afforded on large parallel supercomputers. To exploit the full computational power of these machines a scalable parallel algorithm for the resolution of the equations must be implemented. The details of the parallelization strategy that has been chosen to numerically integrate the Vlasov equation (the most demanding equation in terms of computational resources) can be found in [4].

5. Numerical tests on the hybrid-Vlasov code

In order to discuss the applications of the hybrid-Vlasov code in studying phenomena of relevant interest in plasma physics research, we have evaluated the capabilities of the described scheme by comparing the numerical results obtained by solving several basic problems in collisionless plasma physics to the analytical solutions. First, we discuss propagation and collisionless damping of the linear ion-acoustic waves, taking into account the effects of the finite ratio between ion and electron temperatures T_i/T_e on the frequency and the

damping rate of the oscillations. Then, we describe the behavior of linear Alfvén waves, propagating parallel to the ambient magnetic field and discuss phenomena below and above the ion-cyclotron frequency up to the electron-cyclotron frequency regime including the effects of the electron inertia in the numerical solution of the Ohm's law, as discussed in Section 2.

In all our simulations, the initial distribution of particles is a maxwellian function in the velocity space. As discussed in Section 4, the simulation domain in the physical space is given by $D_x = [0, L_x] \times D_y = [0, L_y]$, while in the velocity space in the ith direction we have $D_v^i = [-v_i^{\max}, v_i^{\max}]$, where $v_i^{\max} = 4.5$–5.0. The time step $\Delta t \simeq 0.005$–0.02 has been chosen in such a way that CFL condition is satisfied. We choose to reproduce numerically physical phenomena that are intrinsically one dimensional in the physical space, in such a way that one can choose to have many grid points in a given spatial direction and few grid points in the other direction.

5.1. Propagation and damping of ion-acoustic waves

Examining the linearized Vlasov electrostatic dispersion relation [21,22], the ion-acoustic solution is found in the range of wave phase velocities $(T_i/m_i) < v_\phi < (T_e/m_e)$ (T_i and T_e are the ion and electron temperatures, respectively), and this is weakly damped if the electrons are warm ($T_e \gg T_i$). The real and the imaginary part of the dielectric function $D(k, \omega)$, under the assumption of weakly damped solutions and maxwellian equilibrium distribution functions, can be written in the following form:

$$D_r = 1 + \frac{1}{k^2 \lambda_{D_e}^2} - \frac{\omega_{\mathrm{pi}}^2}{\omega^2}\left(1 + \frac{3k^2 T_i}{m_i \omega^2}\right) \tag{42}$$

$$D_i = \pi \sum_\alpha \frac{\omega_{p_\alpha}^2}{k^2}\left(\frac{m_\alpha}{2\pi T_\alpha}\right)^{1/2} \frac{m_\alpha}{T_\alpha}\frac{\omega}{k} \exp\left[-\frac{\omega^2 m_\alpha}{2k^2 T_\alpha}\right] \tag{43}$$

where $\alpha = i, e$ indicates ions and electrons, respectively and ω is the real part of the frequency. The expression for ω is found solving for the zeros of D_r:

$$D_r = 0 \Rightarrow \omega^2 = \frac{k^2 T_e}{2m_i(1 + k^2 \lambda_{D_e}^2)}\left[1 + \sqrt{1 + \frac{12 T_i}{T_e}(1 + k^2 \lambda_{D_e}^2)}\right] \tag{44}$$

Taylor expanding for small T_i/T_e, we get:

$$\omega^2 \simeq \frac{k^2 C_s^2}{1 + k^2 \lambda_{D_e}^2}\left[1 + \frac{3T_i}{T_e}(1 + k^2 \lambda_{D_e}^2)\right] \tag{45}$$

where $C_s = \sqrt{T_e/m_i}$ is the so-called ion-sound speed. Finally, in the approximation of large wavelengths ($k^2 \lambda_{D_e}^2 \ll 1$), we obtain:

$$\omega^2 = k^2 C_s^2\left(1 + \frac{3T_i}{T_e}\right) \tag{46}$$

The previous expression gives the modified ion acoustic dispersion containing finite ion temperature effects. The damping rate is obtained by solving the equation:

$$\gamma = -\frac{Di}{\partial D_r/\partial \omega} \tag{47}$$

Due to the fact that in the hybrid approximation electrons are treated as a fluid, particle effects due to electrons, like Landau damping, are ruled out from our model. Therefore, in order to compare the numerical results of the hybrid-Vlasov code to the analytical solution of the Vlasov dispersion relation, we neglect the contribution of electrons in the expression for D_i (43), i.e. we retain only the ion contribution to the wave damping. Then, using (42) and (43) in (47), we get:

$$\omega_i = -\sqrt{\frac{\pi}{8}}\omega\left[\frac{T_e}{T_i}\left(1 + 3\frac{T_i}{T_e}\right)\right]^{3/2} \exp\left[-\frac{T_e}{2T_i}\left(1 + 3\frac{T_i}{T_e}\right)\right]\left(1 + \frac{6T_i}{T_e(1 + 3T_i/T_e)}\right)^{-1} \tag{48}$$

We study the propagation of linear electrostatic ion-acoustic waves, imposing a spatial perturbation of small amplitude on the initial distribution of particles:

$$\delta n = 1 + \sum_{n=1}^{N} \epsilon \cos(k_n x) \tag{49}$$

where $\epsilon = 10^{-4}$, $N = 10$, $k_n = nk_0$ and $k_0 = (2\pi/L_x)$. The propagation of electrostatic ion-acoustic waves is a one-dimensional problem in phase space (1-D in the physical space and 1-D in the velocity space), consequently we can chose to have variations just in the $x - v_x$ space. The length of the simulation interval in the physical space is chosen $L_x = 100\pi$, while the number of grid points is $N_x = 128$. In the velocity space, we have chosen $Nv_x = 40$. The time evolution of the system is followed up to $t_{\max} = 200$. The electric field is evaluated numerically at each time step through Eq. (15), where electron skin depth effects have been neglected ($d_e = 0$).

The dependence of the oscillation frequency ω on the wave number k, is plotted in Fig. 1, for two different values of the ratio T_i/T_e. At the top in the figure, the case of cold ions ($T_i/T_e = 0.01$) is displayed. The dashed line represents the analytical prediction (46), where the corrective term $3T_i/T_e$ has been neglected, while the dots indicate the numerical results. As it is clearly seen from the figure, the numerical solution is in very good agreement with the theoretical one and show that the effect of the finite ion temperature is unimportant for this value of T_i/T_e. At the bottom in the same figure, we have decreased the value of the electron temperature ($T_i/T_e = 0.1$) and we consequently needed to retain the correction $3T_i/T_e$ in (46), to obtain a good agreement between numerical and analytical solution.

If one neglects the electron contribution to the wave damping, as in expression (48), the ion-acoustic waves are totally undamped in the approximation of cold ions, while they are subject to strong damping for non-vanishing values of the ratio T_i/T_e. This behavior is displayed in Fig. 2, where the time evolution of the electric field spectral component (mode $n = 10$) is analyzed for two different values of T_i/T_e. As predicted by the linear theory, undamped oscillations are obtained for $T_i/T_e = 0.01$ (at the top in the figure), while a strong dissipation is visible for $T_i/T_e = 0.1$ (at the bottom).

In order to analyze more quantitatively the Landau damping of the ion-acoustic waves, we chose intermediate values for the ratio T_i/T_e, such that the damping rate is not vanishing and at the same time the analytical

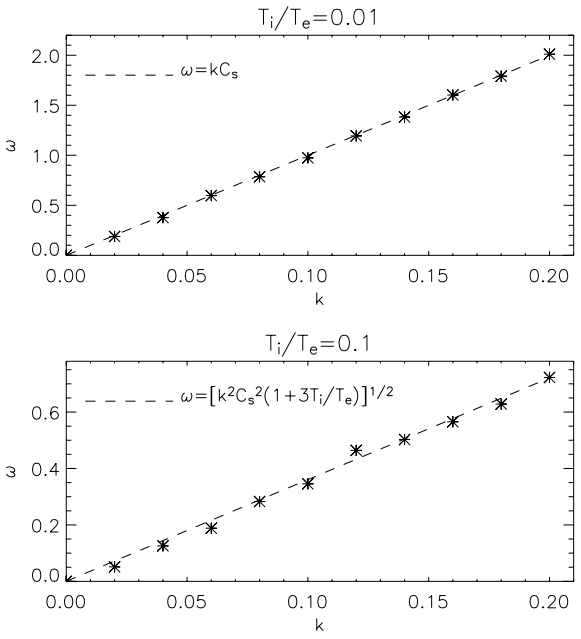

Fig. 1. The dispersion relation for the ion-acoustic waves, for $T_i/T_e = 0.01$ (at the top) and for $T_i/T_e = 0.1$ (at the bottom).

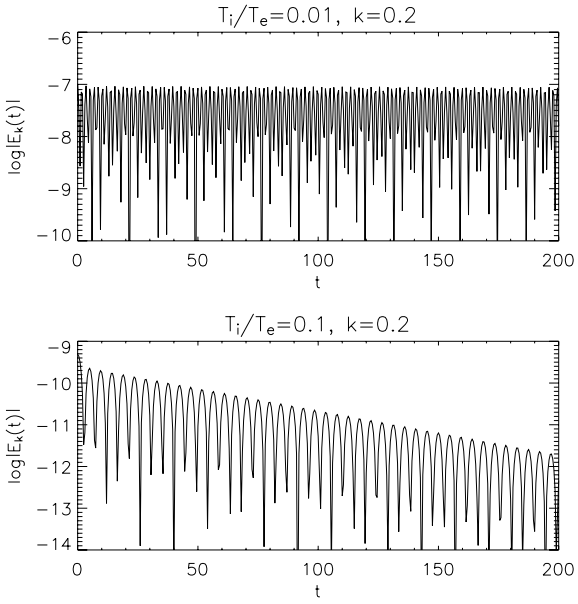

Fig. 2. Time evolution of the electric field spectral component $n = 10$, for two different values of the ratio between ion and electron temperatures; $T_i/T_e = 0.01$ (at the top), $T_i/T_e = 0.1$ (at the bottom).

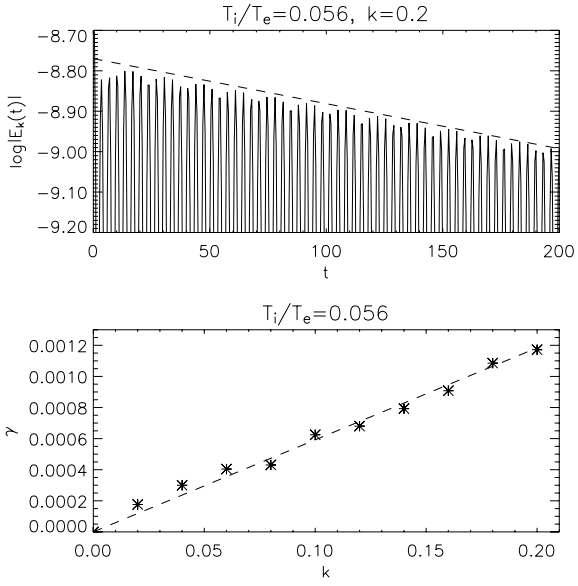

Fig. 3. Time evolution of the electric field spectral component $n = 10$, for $T_i/T_e = 0.056$ (at the top); dependence of the damping rate γ on the wave number k (at the bottom).

solution (48) (or more precisely the Taylor expansion in (45)) is still valid. Then, the time behavior of the electric field is investigated for $T_i/T_e = 0.056$ (Fig. 3) and for $T_i/T_e = 0.048$ (Fig. 4). At the top in both figures, we show the evolution of the mode $n = 10$; the dashed line represents the theoretical prediction for wave damping in Eq. (48). At the bottom, the dependence of the damping rate γ on the wave number k is plotted. The dashed lines represents the analytical expression for the damping rate (48), while the dots are the numerical solutions. As it can easily be seen from the figure, in both cases we observe good agreement between numerical and analytical solutions.

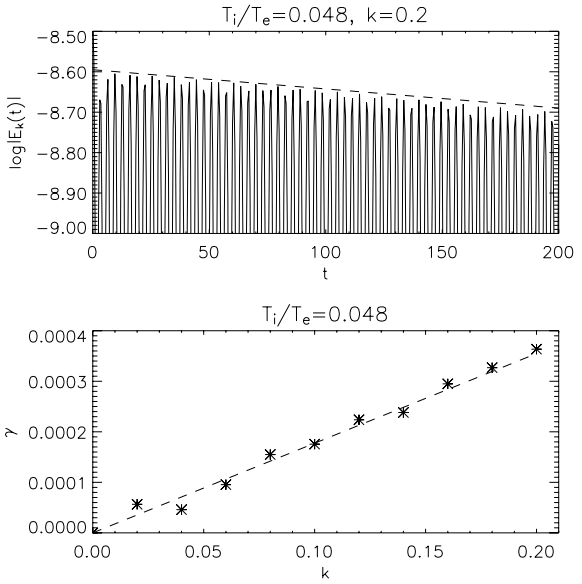

Fig. 4. Time evolution of the electric field spectral component $n = 10$, for $T_i/T_e = 0.048$ (at the top); dependence of the damping rate γ on the wave number k (at the bottom).

5.2. Waves parallel to the ambient magnetic field

In this section, we describe the propagation of elliptically polarized small amplitude Alfvén waves. In particular, we analyze in detail phenomena below and above the ion-cyclotron frequency. We test the hybrid Vlasov code from the low frequency MHD regime up to the range of frequency of the so-called whistler modes, where the effects of electron inertia play a crucial role. To obtain the analytical linear solution for the propagation of these waves, we consider the electron and ion equations of motion coupled to the continuity equation and to Faraday equation:

$$m_\alpha n \frac{\mathrm{d}\mathbf{v}_\alpha}{\mathrm{d}t} = -en\left(\mathbf{E} + \frac{\mathbf{v}_\alpha \times \mathbf{B}}{c}\right) - \nabla P_\alpha; \quad P_\alpha = nT_\alpha; \quad \alpha = e, i \tag{50}$$

$$\frac{\mathrm{d}n}{\mathrm{d}t} + \nabla \cdot (n\mathbf{v}_\alpha) = 0; \quad \frac{1}{c}\frac{\partial \mathbf{B}}{\partial t} = -\nabla \times \mathbf{E}; \quad n_i \simeq n_e \equiv n \tag{51}$$

By linearizing these equations in dimensionless form (see Eq. (6) for characteristic quantities) in the limit of parallel propagation along a uniform magnetic field $\mathbf{B} = B_0\mathbf{e}_x$, we get the following dispersion relation:

$$\omega^2 = \frac{1}{2}\left\{\frac{k^2}{1+k^2d_e^2}\left(2 + \frac{k^2}{1+k^2d_e^2}\right) \pm \sqrt{\frac{k^4}{(1+k^2d_e^2)^3}\left(4k^2 + \frac{k^4}{1+k^2d_e^2}\right)}\right\} \tag{52}$$

where we have taken $B_0 = 1$ and $k = k_x$. Here, the minus/plus sign refers to the L/R branch, which saturate at $\omega = \Omega_{ci}$ and $\omega = \Omega_{ce}$, respectively. We have tested our hybrid-Vlasov code in the parallel propagation, low plasma β limit, by taking at the initial time the normal modes, small amplitude solution of the linearized equations:

$$\delta B_z = \sum_{n=1}^{N} \epsilon \cos(k_n x); \quad \delta B_y = -\sum_{n=1}^{N} \frac{[1 - v_{\phi_n}^2(1 + k_n^2 d_e^2)]}{k_n v_{\phi_n}} \epsilon \sin(k_n x);$$

$$\delta u_z = -\sum_{n=1}^{N} \frac{\epsilon}{v_{\phi_n}} \cos(k_n x); \quad \delta u_y = \sum_{n=1}^{N} \frac{[1 - v_{\phi_n}^2(1 + k_n^2 d_e^2)]}{k_n v_{\phi_n}^2} \epsilon \sin(k_n x) \tag{53}$$

where $\epsilon = 10^{-5}$, $v_\phi = \omega/k$, $k_n = nk_0$ and $k_0 = 2\pi/L_x$. Eq. (15) with $d_e^2 = 1/100$ has been used to evaluate numerically the electric field at each time step.

It is easily seen from Eq. (52) that both the right and the left branches propagate with phase velocity $v_\phi = u_A$ (= 1 in dimensionless units), in the limit of large wavelengths ($k \to 0$). The numerical dispersion relation has been then compared with the theoretical prediction for small wave numbers ($L_x = 140\pi$) and the results are shown in Fig. 5. The dashed line in the figure represents the Aflvén dispersion relation, which is in very good agreement with the numerical results, indicated by dots.

The numerical results for higher values of the wave number k are shown in Fig. 6 for two simulations both with a uniform magnetic field along x-axis, $\mathbf{B} = B_0\mathbf{e}_x$ with $B_0 = 1$, and with $u_{th}/u_A = 0.01$, $m_i/m_e = 100$ and $L_x = 10\pi$ (left panel) $L_x = 1.68\pi$ (right panel). The left panel is obtained by taking Eq. (53) as initial condition with ω given by Eq. (52) taking the minus solution corresponding to L-modes. The right panel is obtained in the same way taking the other solution (plus sign) from Eq. (52) corresponding to R-modes. The results show that at low frequency, $\omega \ll 1$, we get in both cases the well known Alfvén branch $\omega = k$ (recall that $u_A = 1$), which tends to saturates at the ion gyrofrequency for the L-mode (left panel) and at electron gyrofrequency for the R-mode (right panel) going through the whistler regime. The corresponding eigenfunctions for each wave number (not shown here) are also in very good agreement with linear theory during all the simulation time.

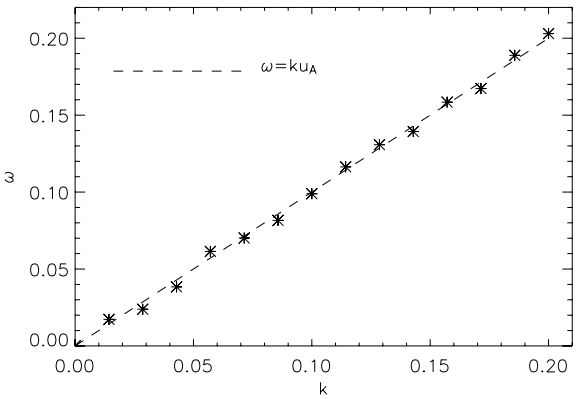

Fig. 5. The dispersion relation in the large wavelength limit.

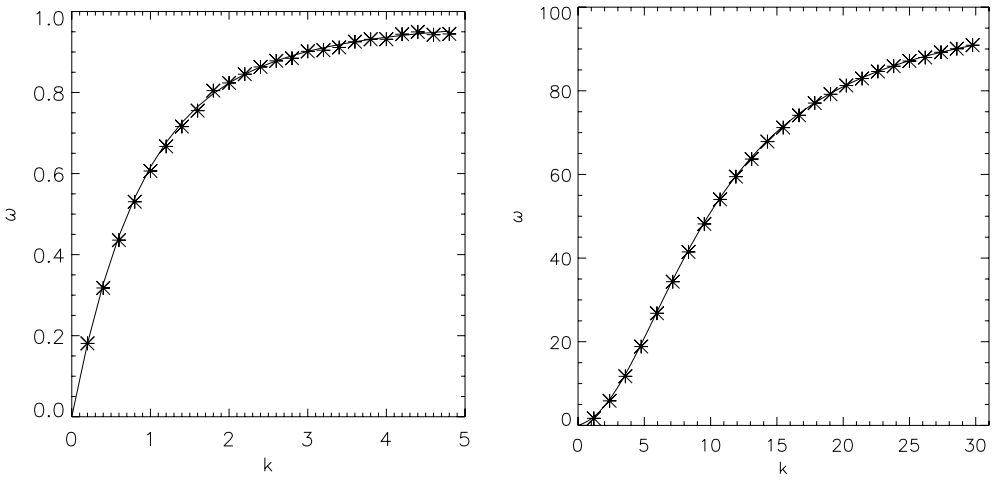

Fig. 6. The L- and R-mode dispersion relation, Eq. (52), left and right panel, respectively. Here $\Omega_{ci} = 1$ and $\Omega_{ce} = 100$.

6. Parametric instability

We consider now the well known decay instability of parallel Alfvén waves propagating in a collisionless plasma. This instability produces a forward propagating acoustic wave and a backward Alfvén wave with a wave number smaller than that of the pump. This is therefore an excellent test for a *low noise* Vlasov code since it couples magnetic Alfvénic perturbations to density fluctuations. In order to limit the computational time, we consider here the dispersionless limit of parallel propagating Alfvén waves in a warm ion plasma in a background of massless, cold electrons ($d_e = 0$, $P_e = T_e = 0$). In this case the Ohm's law, Eq. (54), reduces to

$$\mathbf{E} + (\mathbf{u} \times \mathbf{B}) = \frac{1}{n}(\mathbf{j} \times \mathbf{B}) \tag{54}$$

We use the Alfvén velocity u_A as the characteristic velocity ($u \equiv$ dimensionless velocity), $\overline{P}$ as a characteristic ion pressure and the parameter α as the Alfvén to thermal velocity ratio:

$$u = v/u_A; \quad \overline{P} = \bar{n} m_i u_A^2; \quad \alpha = u_A^2/u_{th}^2$$

where P, v and u indicate ion quantities. The magnetic, velocity and density perturbations are defined as

$$\delta B_y = \delta B_0 \cos(k_0 x); \quad \delta B_z = -\delta B_0 \sin(k_0 x) \tag{55}$$

$$\delta u_y = ((k_0 - z_0)/k_0)\delta B_y; \quad \delta u_z = ((k_0 - z_0)/k_0)\delta B_z \tag{56}$$

$$\delta n = \text{random noise} \tag{57}$$

and the dimensionless ion distribution function reads

$$f = n \exp\left\{-\frac{1}{2}[(u_x^2 + (u_y - \delta u_y)^2 + (u_z - \delta u_z)^2]\alpha\right\} \tag{58}$$

Therefore, in agreement with our definition in Eq. (56), the mean (fluid) velocity is given by

$$U_x = \int f u_x \, du_x \, du_y \, du_z = 0$$

$$U_y = \int f u_y \, du_x \, du_y \, du_z = \delta u_y$$

$$U_z = \int f u_z \, du_x \, du_y \, du_z = \delta u_z$$

From the definition of the total pressure, $P = (P_{xx} + P_{yy} + P_{zz})/3$, where

$$P_{ii} = \int f (u_i - U_i)^2 \, du_x \, du_y \, du_z; \quad i = x, y, x$$

we get $P_{xx} = P_{yy} = P_{zz} = \alpha^{-1}$ and so $P = \alpha^{-1}$. Using the tilde and bar symbols for dimensional and characteristic quantities, we calculate the plasma β as

$$\beta = \frac{8\pi \widetilde{P}_{isotr}}{\widetilde{B}_0^2} = 8\pi \frac{P}{B_0^2} \frac{\overline{P}}{\overline{B}_0^2} = 2 \frac{P}{B_0^2} \frac{4\pi \bar{n} m_i u_A^2}{\overline{B}_0^2} = 2 \frac{P}{B_0^2}$$

which gives $\alpha = 2/\beta$ since the ambient magnetic field is homogeneous and normalized to unity, $B_0 = 1$.

We take a forward-propagating right-hand polarized Alfvén wave of amplitude $\delta B_0 = 0.5$ and wave vector $k_0 = 0.408$, corresponding to a simulation domain $L_x = 2\pi \times m/k_0 \simeq 123.2$, with $m = 8$. Furthermore, $z_0 = 0.515$ and $\beta = 0.45$ which gives $\alpha = 4.44$ to be used for the ion distribution function, Eq. (58) corresponding to a dimensionless thermal ion velocity $u_{th} \simeq 0.5$. As a result the ion Larmor radius is $\rho_L = u_{th}/\Omega_{ci} = 0.5$, to be compared to the initial Alfvén wave wavelength $\lambda_0 \simeq 15$.

The ion Vlasov, cold fluid electron equations are integrated on a uniform grid (x, v_x, v_y, v_z) with $N_x = 64$ and $(2Nv_x + 1) \times (2Nv_y + 1) \times (2Nv_z + 1) = 61^3$ phase space mesh points with $-v_i^{max} \leqslant v_i \leqslant v_i^{max}$, $v_i^{max} = 4.5$, $i = x, y, z$. The time step is $\Delta t = 0.02$. The time evolution of the system is followed up to $t_{max} = 960$. Identical results to those presented in the following have been obtained by varying the grid mesh points, in particular

with $N_x = 128$ and $N_x = 256$ in order to check that the growth rate of the instability is not affected by dissipative and/or dispersive numerical effects.

In Fig. 7 we show the time evolution of the modulus of the Fourier amplitude of the initially excited y-component of the magnetic field, $\delta B_y(m = 8)$, of the most unstable density mode $\delta n(m = 13)$ corresponding to the excited forward acoustic wave and of the most unstable magnetic mode, $\delta B_y(m = 5)$, corresponding to the excited backward Alfvén wave. We see that both modes grow exponentially with the same growth rate, $\gamma = 0.02$, and saturate at nearly $t = 550$ due to ion trapping effects.

This is in agreement with the theoretical analysis which predicts the acoustic mode $m = 13$ and the back scattered Alfvén wave $m = 5$ as the most unstable excited wave by the decaying instability. We underline that our results are not influenced by dissipative grid effects since the same value for the growth rate is obtained when varying the numerical mesh grid.

In Fig. 8 we show, as an example, the ion distribution function f in the (x, v_x) phase space for v_y and v_z values slightly smaller or comparable to the ion thermal velocity and at different times. We see that very soon, $t = 60$, the distribution function is already significantly influenced by kinetic effects. At $t = 540$ the ion d.f. is strongly perturbed by particle trapping already showing some non-collisional heating similar to what found in Ref. [23] in the case of high frequency longitudinal waves in a magnetized plasma. Finally, other two runs with $\beta = 0.9$, $\beta = 0.225$ and $\beta = 0.05$ give $\gamma = 0.009$, $\gamma = 0.038$ and $\gamma = 0.11$, respectively. The last one,

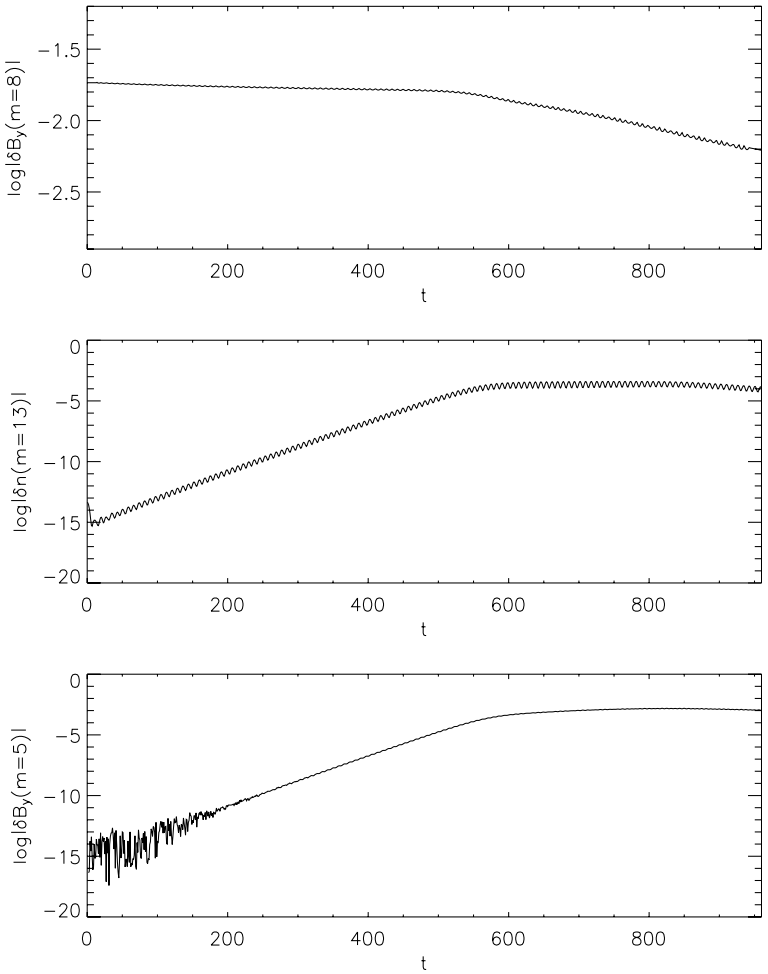

Fig. 7. The time evolution of the (smoothed in time) modulus of the Fourier amplitude $\delta B_y(m = 8)$, $\delta n(m = 13)$ and $\delta B_y(m = 5)$, respectively. For the sake of clearness, a smoothing function has been applied to the first curve of the $m = 8$ Alfvén mode in order to eliminate high frequency oscillations.

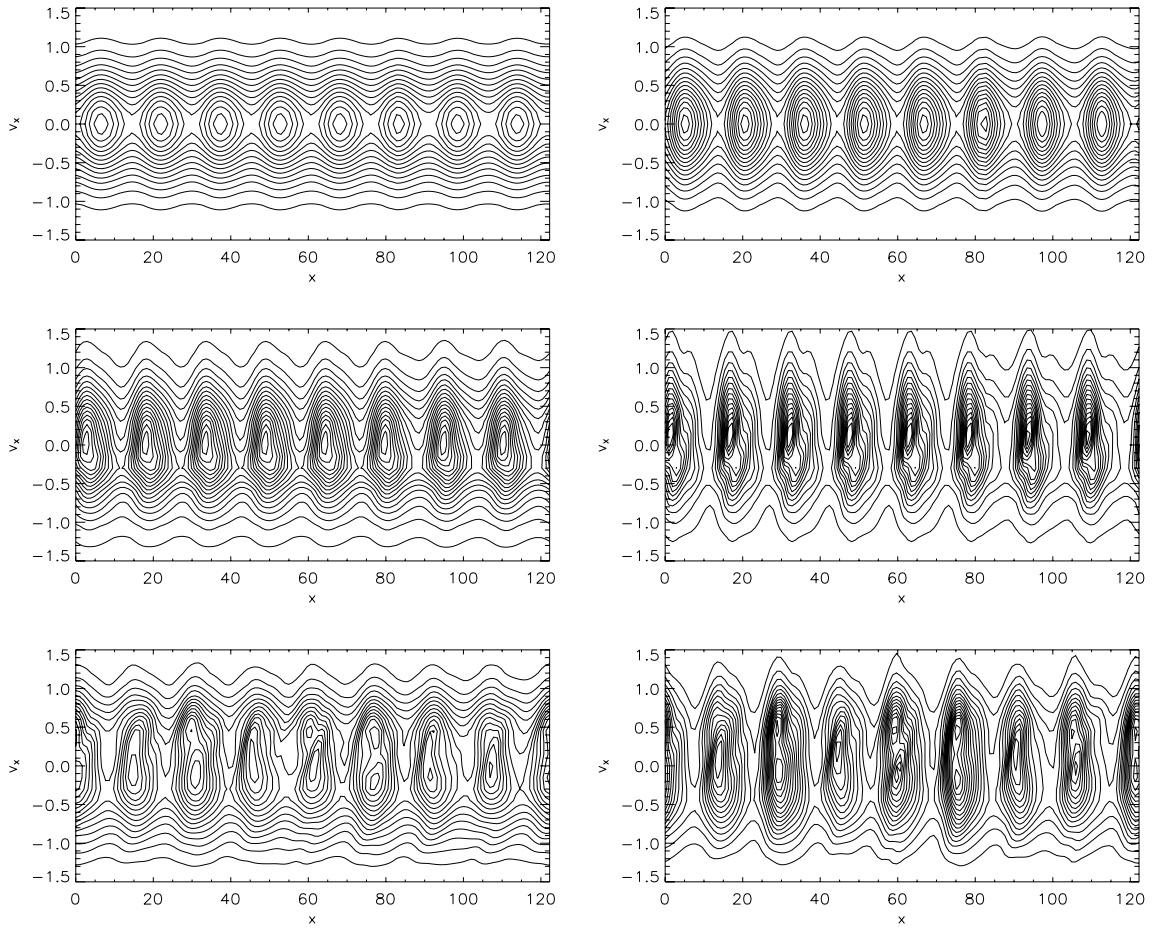

Fig. 8. The ion d.f. in the (x, vx) phase space at $v_y = v_z = 0.3$, first column and at $v_y = 0.3$, $v_z = 0.9$, second column. First, second and third row refers to $t = 0, 60, 540$, respectively.

$\beta = 0.05$, is in good agreement with a two-fluid calculation, where we found $\gamma_{2f} = 0.12$. The agreement with the two-fluid model gets worse as β increases, as for example in the case of $\beta = 0.45$ where the two-fluid models gives $\gamma_{2f} = 0.055$, more than twice the growth in the hybrid-Vlasov case.

7. Summary

In this paper we presented a new hybrid-Vlasov algorithm which combines the standard splitting techniques used for Eulerian Vlasov codes together with the CAM method for the calculation of the electromagnetic fields developed for PIC simulations. We give, to our knowledge, a new expression for the Ohm's law where electron inertial effects are included. Such effects are in general neglected in the kinetic hybrid simulations. Several analytical benchmarks are presented here to test the accuracy of the code. Our model allows to study, generally speaking, kinetic plasma problems where the dynamics is basically driven by the ions in a large frequency interval, from the low frequency Alfvén regime of the MHD one-fluid model up to the high frequency whistler regime of Electron-MHD. The use of the CAM approximation allows us to reduce the computational cost for the solution of the Vlasov–Maxwell system with respect to the standard splitting techniques used in Ref. [4].

Acknowledgments

The authors gratefully acknowledge useful discussions with Prof. P. Veltri and Prof. F. Pegoraro. This work was supported by CINECA, Bologna, Italy.

References

[1] C.Z. Cheng, G. Knorr, J. Comput. Phys. 22 (1976) 330–351.
[2] A.P. Matthews, J. Comput. Phys. 112 (1994) 102–116.
[3] C.k. Birdsall, A.B. Langdon, Plasma Physics Via Computer Simulation, McGraw-Hill Book Co., Singapore, 1985.
[4] A. Mangeney, F. Califano, C. Cavazzoni, P. Travnicek, J. Comput. Phys. 179 (2002) 495–538.
[5] P. Hellinger, P. Trávníček, H. Matsumoto, Geophys. Res. Lett. 29 (2002) 87-1–87-3.
[6] D. Winske, N. Omidi, J. Geophys. Res. 101 (1996) 17287–17304.
[7] D. Nunn, J. Comput. Phys. 108 (1993) 180–196.
[8] A.S. Lipatov, The Hybrid Multiscale Simulation Technology, Springer-Verlag, Berlin, 2002.
[9] S.V. Bulanov, F. Pegoraro, A.S. Sakharov, Phys. Fluids B 4 (1992) 2499.
[10] E. Fijalkow, Comput. Phys. Commun. 116 (1999) 319–328.
[11] E. Fijalkow, Comput. Phys. Commun. 116 (1999) 329–335.
[12] E. Fijalkow, Comput. Phys. Commun. 116 (1999) 336–344.
[13] F. Valentini, P. Veltri, A. Mangeney, J. Comput. Phys. 210 (2005) 730–751.
[14] R. Peyret, T.D. Taylor, Computational Methods for Fluid Flow, Springer-Verlag, New York, 1983.
[15] E. Godlewski, P.A. Raviart, Numerical Approximation of Hyperbolic System of Conservation Laws, Springer-Verlag, New York, 1995.
[16] A. Harten, J. Comput. Phys. 135 (1982) 260–278.
[17] A. Harten, J. Comput. Phys. 131 (1986) 3–46.
[18] A. Harten, J. Comput. Phys. 131 (1982) 247–250.
[19] Randall J. Leveque, SIAM. J. Numer. Anal. 33 (1996) 627–665.
[20] B. Van Leer, J. Comput. Phys. 23 (1976) 263–275.
[21] N.A. Kraal, A.W. Trivelpiece, Principles of Plasma Physics, San Francisco Press, San Francisco, 1986.
[22] F.F. Chen, Plasma Physics and Controlled Fusion, Plenum press, New York, 1984.
[23] F. Califano, M. Lontano, Phys. Rev. E 67 (2003) 056401-1–056401-5.